Study on internal to surface fingerprint correlation using optical coherence tomography and internal fingerprint extraction

Luke Nicholas Darlow
James Connan

Study on internal to surface fingerprint correlation using optical coherence tomography and internal fingerprint extraction

Luke Nicholas Darlow[a,b,*] and James Connan[a]
[a]Rhodes University, Computer Science Department, Prince Alfred Street, Grahamstown, Eastern Cape 6139, South Africa
[b]Modelling and Digital Science, Council for Scientific and Industrial Research, Meiring Naude Road, Pretoria, Gauteng 0184, South Africa

Abstract. Surface fingerprint scanners are limited to a two-dimensional representation of the fingerprint topography, and thus, are vulnerable to fingerprint damage, distortion, and counterfeiting. Optical coherence tomography (OCT) scanners are able to image (in three dimensions) the internal structure of the fingertip skin. Techniques for obtaining the internal fingerprint from OCT scans have since been developed. This research presents an internal fingerprint extraction algorithm designed to extract high-quality internal fingerprints from touchless OCT fingertip scans. Furthermore, it serves as a correlation study between surface and internal fingerprints. Provided the scanned region contains sufficient fingerprint information, correlation to the surface topography is shown to be good (74% have true matches). The cross-correlation of internal fingerprints (96% have true matches) is substantial that internal fingerprints can constitute a fingerprint database. The internal fingerprints' performance was also compared to the performance of cropped surface counterparts, to eliminate bias owing to information level present, showing that the internal fingerprints' performance is superior 63.6% of the time. © 2015 SPIE and IS&T [DOI: 10.1117/1.JEI.24.6.063014]

1 Introduction

The authenticity and performance of biometrics such as fingerprints are under constant scrutiny. Matsumoto et al.[1] highlighted the lack of fingerprint authenticity detection. Although liveness detection has come a long way,[2,3] there is nevertheless a limit to surface fingerprints.

The inherent limit is that the current surface fingerprint scanning standard provides a two-dimensional (2-D) fingerprint representation that accommodates fingerprint spoofing,[1,4] thus requiring sophisticated methods for authenticity detection.[3] The surface scanners are touch-based, and thus, introduce distortion.[5] Surface fingerprint skin is also prone to damage.

Solutions to mitigate surface fingerprint disadvantages have been developed. Three-dimensional (3-D) surface fingerprint imaging with 3-D to 2-D unwrapping,[6] fingerprint distortion removal,[5] fingerprint recognition in low-quality fingerprint images,[7] fingerprint enhancement,[8] and fingerprint liveness detection[3] are all noteworthy contributions to this task. However, a solution exists that is able to compensate simultaneously for all the deficiencies of the surface fingerprint: the internal fingerprint.

There is a layer of skin, known as the papillary junction, that has the same topography as the surface. Thus, the surface and internal fingerprint have the same structure.[9] Owing to the relative reflectivity of the papillary junction to the epidermis, the upper edge of the papillary junction contains the most pertinent internal fingerprint information.

The imaging of subsurface layers of skin is carried out using a tool known as optical coherence tomography (OCT).[10] OCT has become known as a powerful and non-invasive biomedical imaging tool. It is touchless and can image the papillary junction in high-resolution 3-D. OCT is subject to signal-degrading speckle noise that originates from reflective elements of roughly the same size as the imaging wavelength.[11] An OCT volume consists of a series of image slices (known as B-scans) that consist of a series of one-dimensional (1-D) signals (known as A-lines). A-lines are columns in a B-scan.

Various successful attempts[12–16] have made use of OCT to image the internal fingerprint. However, these works usually define the location of the papillary junction manually. Furthermore, most employed either simple *en face* slice averaging (over a static region) or used a single *en face* slice for internal fingerprint extraction. Although the use of a glass slide during the scanning process (as was the case in the work of Bossen et al.[12]) does stabilize the location of the papillary junction to a relatively fixed depth, it mitigates the touchless capability of OCT. This earlier research lacked automatic internal fingerprint zone detection and was technically inefficient regarding internal fingerprint extraction. The result was low-quality internal fingerprints. An improved approach was developed by Khutlang and Nelwamondo:[17] Novelty detection was used to locate the papillary junction. Compared to human observers, this technique performed well. However, their method required B-scan images to be processed to reduce noise and the dataset for testing was small.

*Address all correspondence to: Luke Nicholas Darlow, E-mail: LDarlow@csir.co.za

Darlow et al.[18] used heuristic techniques to detect the papillary junction upper edge and developed an improved technique for *en face* slice averaging. Slice averaging consisted of averaging pixels over a fixed region (surrounding the detected fingerprint zone) in each B-scan. Akhoury and Darlow[19] applied an automatic papillary junction detection approach and mapped the obtained 3-D papillary junction coordinates to a 2-D fingerprint representation. In addition, internal fingerprint zone detection was accomplished by Darlow et al.:[20] the approximate location of the papillary junction was detected by applying *k*-means clustering to A-line local maxima; a fine-tuning procedure was applied to localize the papillary junction upper edge (i.e., the internal fingerprint zone). However, the fingerprints obtained in all cases were not quantitatively tested for correlation with their surface counterparts, nor was the dataset large enough to conclude robustness with regard to internal fingerprint extraction.

The research presented here is an improvement on, and conglomeration of, the above-mentioned works. Internal fingerprint zone detection is an improvement as it uses fuzzy *c*-means to improve clustering performance, uses better cluster result postprocessing, and improves upon the fine-tuning procedure through the application of Sobel and Feldman[21] edge detection. The fingerprint extraction approach is an improvement on the work by Darlow et al.[18] in that it is localized to individual A-lines, instead of being fixed on a B-scan basis.

No research has been undertaken to show the correlation between surface and internal fingerprints in a decisive quantitative manner. This is necessary to provide evidence that (1) the internal fingerprint is a viable replacement for the surface fingerprint and (2) the internal fingerprint can be incorporated into legacy fingerprint databases.

To accomplish this, an internal fingerprint extraction algorithm is developed in this research, tested, and applied to OCT fingertip scans. The approach is novel and technically advanced in its use of computer vision techniques. Although the origin of this algorithm has its roots in earlier works, the deviations, improvements, and consequent additions are significant.

This algorithm uses clustering and image-enhancement procedures to detect the upper edge of the papillary junction with high accuracy. Following this, the papillary junction undulation zone is described in a local fashion for internal fingerprint extraction.

This paper is structured as follows. The internal fingerprint extraction algorithm is presented in Sec. 2. The experimental setup is detailed in Sec. 3, and the results obtained are exhibited in Sec. 4. The conclusions are drawn and future work is suggested in Sec. 5.

2 Internal Fingerprint Extraction Algorithm

Internal fingerprint extraction consists of two main parts: fingerprint zone detection and extraction. Zone detection uses fuzzy *c*-means clustering to approximate the location of the papillary junction (i.e., the internal fingerprint zone). Edge detection is used to further localize this location. The following section details the approach developed for internal fingerprint zone detection.

2.1 Internal Fingerprint Zone Detection

Figure 1 is an overview flowchart describing the internal fingerprint extraction algorithm. The data acquisition process and respective resolution constraints are explained in Sec. 3. No glass slide was used during fingertip scanning as this mitigates the touchless advantage of OCT. Figures 1(a) and 1(b)
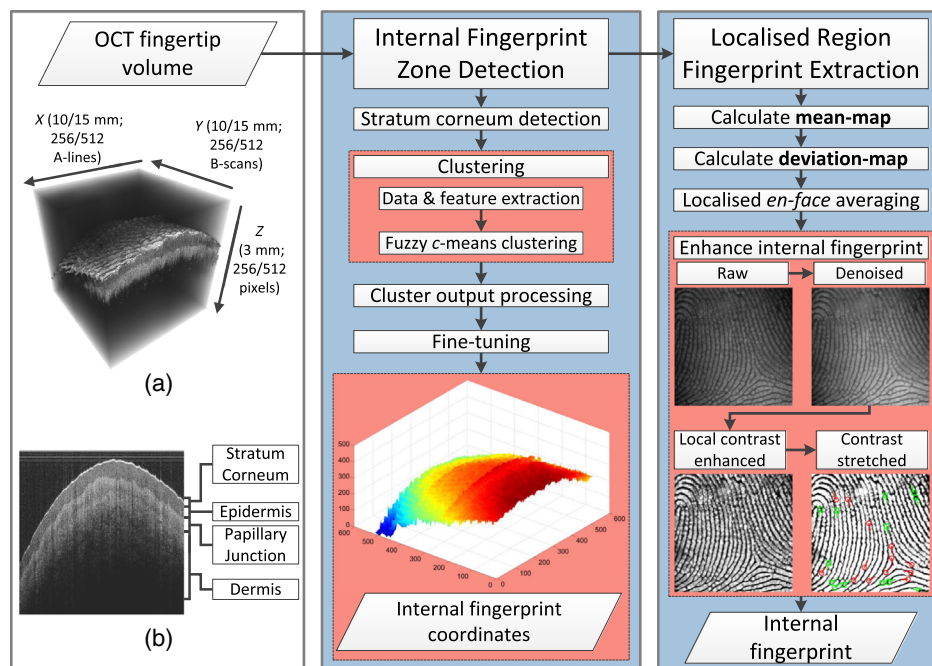
Fig. 1 The novel internal fingerprint extraction algorithm. (a) A typical optical coherence tomography (OCT) fingertip scan with resolution constraints (see Sec. 3), while (b) identifies the layers of skin by their relative reflectivity in a single OCT scan image (B-scan).

are indicative of the visible curvature of the scanned fingertips.

There is an intensity depth dependency roll-off problem inherent in OCT scans of a curved object. Regions further from the scanner have lower intensity, and the natural finger curvature makes internal fingerprint zone detection complex. This research endeavors to detect the internal fingerprint zone in unprocessed, touchless OCT fingertip scans.

To do so, fuzzy c-means clustering is applied to *en face* 1-D intensity signals (known as A-lines, exemplified in Fig. 2) for internal fingerprint zone detection. This information is used to define *en face* localized regions for each A-line over which to average pixel intensities for the 2-D internal fingerprint. Following this, the internal fingerprint is enhanced.

Fuzzy c-means[22] clustering is applied to internal fingerprint zone detection as: it suits the task of papillary junction detection, has been implemented and tested in various scenarios, and is highly robust against outliers. The outlier detection capacity of fuzzy c-means is used by setting a high threshold for cluster membership [Eq. (1)] and duly accommodated for by coordinate interpolation.

Clustering requires input data and descriptive features. A number (n) of intensity local maxima in each A-line are extracted as data. Examples of this data are the (green) dots in Fig. 2. Refer to this graph for visual descriptors of the following features:

1. Relative distance to the stratum corneum: Black arrows in Fig. 2. The stratum corneum is detected as detailed in Fig. 3(a). The distances from this estimate—the dashed (green) line in Fig. 2—to the extracted data points are normalized on a B-scan basis by estimating the average (median) distance between the two strongest peaks in all A-lines in the respective B-scan.

2. Relative intensity: Height of the (green) dots in Fig. 2. The second strongest local maximum usually (but not always) corresponds with the papillary junction. The median (on a B-scan basis) of these maxima is used to normalize this feature. The median is used as it is robust regarding outliers.

3. Peak width: Bottom (blue, above peaks) arrows in Fig. 2. Calculated as twice the distance from the data point to the next upper local minimum.

4. Standard deviation: Top (purple, above peaks) arrows in Fig. 2. Calculated over the region defined by the peak width.

5. Gradient: Measured at **X**, half the distance between the data point and the next upper local minimum.

It is the normalization of the distance and intensity features that adjusts fingertip curvature and roll-off. Cluster membership is defined by

$$T(c) = \min\left(\frac{m}{c}, \text{threshold}\right), \qquad (1)$$

where $m > 1$ is the multiplication factor, c is the number of clusters, and threshold is the maximum membership value and is set to 0.9. Threshold exists to ensure at least some membership in fringe cases (i.e., when m is high and c is low). m was set to 1.6 for this research, although it must be noted that this parameter is not sensitive. If a data point does not have a membership of at least T in any of the c clusters, it is an outlier. A large number of outliers must not be interpreted as poor performance. Instead, it serves to ensure strong cluster membership. Figure 3(b) is an example of clustering output.

The cluster best describing the internal fingerprint zone is determined by comparing each cluster to the estimate used for relative distance normalization. The data contained in the chosen cluster are denoted as C.

Owing to the imposed requirement of strong cluster membership, it is entirely possible that A-lines may contain no data within C. Interpolating missing data is thus required.

The inpaint_nan[23] interpolation algorithm is used to calculate missing values in C. A median filter is applied to the coordinates to reduce anomalies. The resultant coordinates are denoted as PC. The process followed is exhibited in Fig. 4.

PC describes the center of the papillary junction only and is thus inefficient at capturing the internal fingerprint undulations. PC is fine-tuned into papillary junction upper-edge coordinates (denoted as P). P describes the internal fingerprint zone entirely. Fine-tuning involves processing small image regions. This region is exemplified as the region between the (red and blue) lines in Figs. 3(c) and 3(d). These image regions contain the papillary junction upper edge.
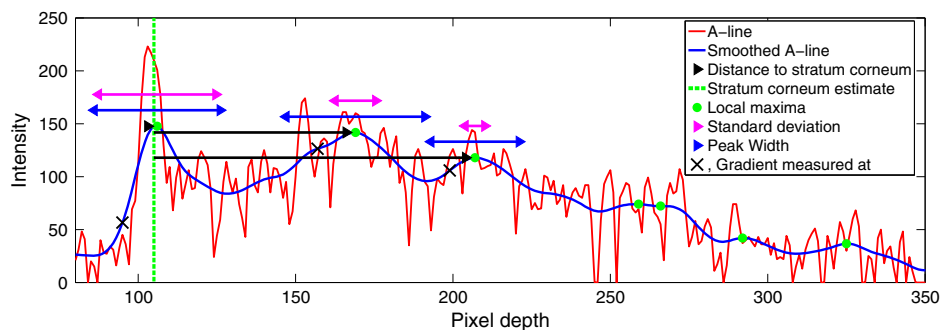

Fig. 2 A region of interest in a single one-dimensional A-line intensity profile. The features extracted for fuzzy c-means clustering are exemplified herein.
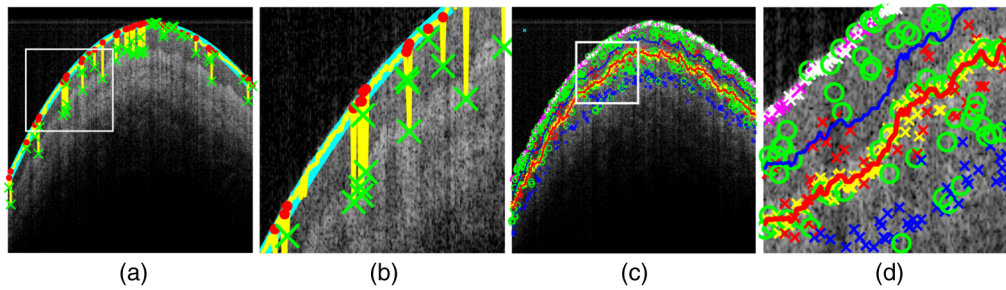
Fig. 3 Clustering process. (a) Exemplifies stratum corneum detection: the thin (yellow) line indicates the local maxima estimates closest to the previous B-scan's stratum corneum and a polynomial fitted to strong data points [i.e., the thick (cyan) line]; the (green) crosses are outliers; and the (red) dots are corrected outliers. (b) An example of output clusters: different color/marker combinations are different clusters; large (green) circles encircle the outliers; and the bottom (red) and top (green) lines show the region extracted for fine-tuning (Fig. 5).
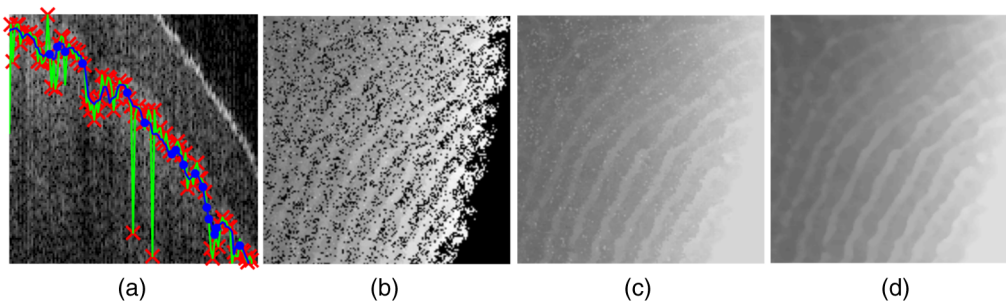

Fig. 4 Cluster result processing. (a) A region of interest in a B-scan: the (red) crosses are cluster results, (b) the (blue) dots are interpolated values; (c) the deviating (green) line is prior to median smoothing; and (d) the smooth (blue) line is after smoothing. (b), (c), and (d) are *en face* perspectives of the papillary junction center coordinates before interpolation, after interpolation, and after smoothing, respectively.

The optimized blockwise nonlocal means (OBNLM) speckle filter was shown by Darlow et al.[24] to perform well regarding OCT fingertip scans and is applied in succession to the regions. Local intensity normalization is used to alleviate the effects of the curvature roll-off problem. The Sobel and Feldman[21] operator detects the horizontal edges, and unsharp masking enhances them. The thresholded result is processed for edge coordinates and used to adjust PC, yielding P. This process is demonstrated in Fig. 5. PC and P are illustrated as the bottom (cyan) and top (green) lines in Fig. 6(a), respectively.

An earlier work by Darlow et al.[20] served as a precursor to this approach. In that work, k-means clustering was used, and a different set of procedures was used for fine-tuning. The novelty of this work is found in the manner in which fuzzy c-means is able to identify outliers, the approach to cluster result postprocessing, and the use of Sobel edge detection for fine-tuning.

Since there should only be a single data point per A-line that corresponds to the papillary junction, and because fuzzy c-means performs well regarding outlier detection, a ratio of $c : n$ where $c > n$ is hypothesized to yield satisfactory results.
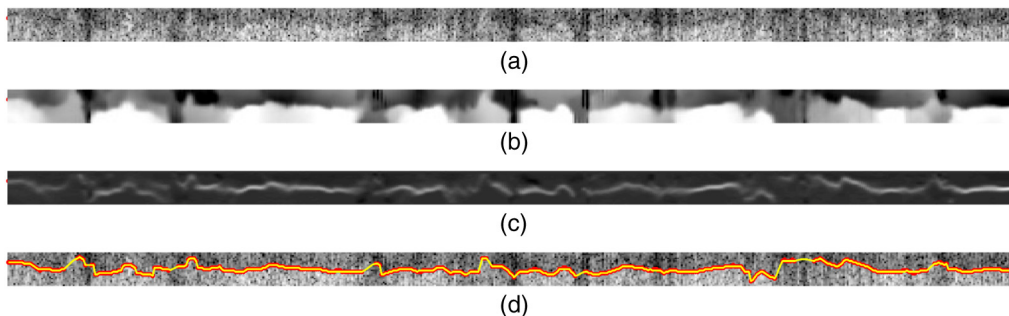
Fig. 5 Fine-tuning process. (a) An example of the small image regions processed for fine-tuning, extracted from between the lines in Fig. 3(b). (b) After the successive application of optimized blockwise nonlocal means (OBNLM) (in three stages) and local normalization. (c) The application of the Sobel operator yields. The edge detected is shown in (d).
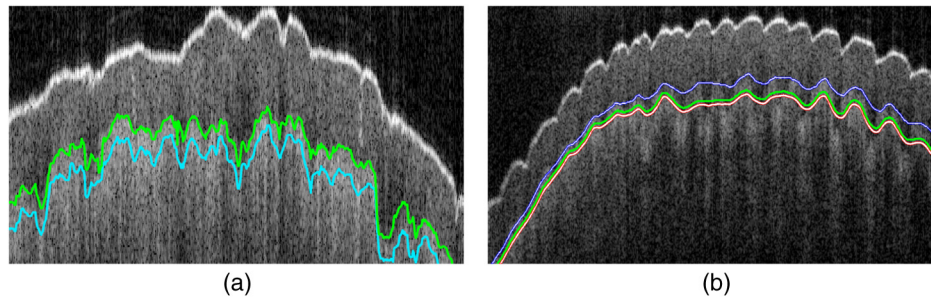
Fig. 6 Adjustments owing to fine-tuning and the localized region for extraction. (a) A region of interest in a B-scan: PC and P are the bottom (cyan) and top (green) lines, respectively. (b) The localized region capturing the internal fingerprint: A-lines are averaged between the top (blue and white) and middle (green) lines, while the bottom (red and white) line is the mean-map used to describe this region. Meano $= 2$, devo $= 3$, and devm $= 5$.

This is shown in Sec. 4. Fingerprint extraction using P is discussed in the following section.

2.2 Localized Internal Fingerprint Extraction

A 2-D *en face* coordinate mean-map and standard deviation-map is calculated from P. These are P convolved with averaging and standard deviation filters, respectively. They are localized to an individual XY pixel and are used to provide statistical evaluations of the papillary junction undulations. The region describing the internal fingerprint starts at the mean-map adjusted by some offset (meano), and ends at the deviation-map multiplied by a constant (devm) and adjusted by some offset (devo). This region is demonstrated in Fig. 6(b) as the region between the middle (green) and top (blue and white) lines.

The statistical evaluation of the fingerprint zone results in resistance toward deviation in the detected zone. Thus, this manner of fingerprint extraction is insensitive to inconsistencies in detection, whether from poor algorithmic performance or deviations introduced owing to coordinate interpolation.

The internal fingerprint is extracted by averaging the pixels in the above-mentioned region. It is enhanced following the procedure outlined in Fig. 7: speckle noise is reduced using OBNLM, contrast is normalized on a local basis, and the intensity values are saturated. The experimental setup, designed to test the correlation between internal and surface fingerprints, and the extraction algorithm are detailed in the following section.

3 Experimental Setup

Fingertips were scanned using a swept-source OCT system (OCS1300SS, Thorlabs). It has a central wavelength of 1325 nm, a spectral bandwidth of 100 nm, an axial scan rate of 16 kHz, and a coherence length of 6 mm. No glass slide was used for stabilization. The depth and resolution of A-lines obtained were set at 3 mm and 512 pixels, respectively. *En face* areas of 10 mm × 10 mm and 15 mm × 15 mm were combined with resolutions of 512×512 pixels and 256×256 pixels. Multiple instances of 10 fingers were scanned, totaling 55 OCT volumes.

P was tested against a ground-truth estimation (G) that was manually performed on a single OCT volume. The papillary junction upper edge (i.e., fingerprint zone) was manually detected. The mean squared error (MSE) and the Hausdorff[25] distance metric (H) were used to assess the performance of the proposed algorithm. The tested range for both n and c is $2:23$. This limit was imposed by the lengthy time taken to process when c and n are high.

The G'MIC[26] image computing library was used for local normalization. All other image-enhancement procedures were carried out in MATLAB.

The volumes obtained were within three subjectively defined categories: (1) small region and bad area (i.e., far from the fingerprint core); (2) small region and good area (i.e., at or near the fingerprint core); and (3) large region and good area. The area- and resolution-based categorization were used to emphasize internal fingerprint performance dependency on the imaged region (i.e., available minutiae).

The Integrated Biometrics Watson Mini (and the IBScanUltimate 1.6.10 software) and the SecuGen Hamster
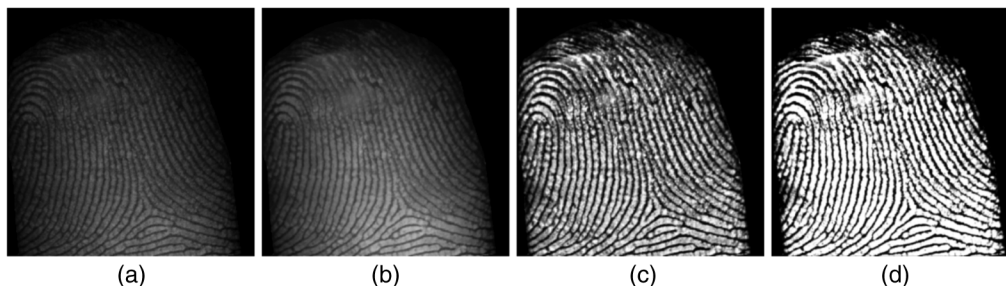
Fig. 7 Internal fingerprint enhancement: (a) an internal fingerprint extracted from the OCT volume using P and the technique shown in Fig. 6; (b) after OBNLM speckle noise reduction; (c) after local contrast normalization; and (d) after global intensity saturation.

Plus (and the device software) were used to capture surface fingerprints. Eight surface fingerprints were provided by each of these scanners, resulting in 16 full-sized corresponding surface scans for each finger.

The NIST[27] fingerprint minutiae extractor (*mindtct*) and matching algorithm (*bozarth3*) were used to evaluate internal to surface fingerprint correlation and internal fingerprint cross-correlation. Since high-surface fingerprint quality is 500 ppi, the internal fingerprints were scaled to correspond to this. Regarding fingerprint quality evaluation, the NIST fingerprint score (NFIQ) and the orientation certainty level (OCL)[28] were calculated for all fingerprints. NFIQ is a category-based score that ranges from 1 (best) to 5 (worst) and is dependent on information level (i.e., number and quality of minutiae points), while lower OCL scores indicate better energy concentration along the dominant ridge-valley orientation.

In order to provide a thorough qualitative assessment of the performance of the internal fingerprint, some reference point must be given. To provide such a reference point, three conventional surface fingerprints were obtained (using the Integrated Biometrics Watson Mini) and cropped to correspond each internal fingerprint. This process mitigated the potential for bias based on fingerprint region size (and, thus, number of minutiae present for matching) and locality (i.e., orientation about the center of the fingerprint). Where necessary, comparisons were made between the internal and the surface-region-of-interest-fingerprints (SROI-fingerprints).

The capture and subjective division of OCT fingertip scans into three categories are advantageous in the comparison between internal fingerprints and SROI-fingerprints. Testing different fingerprint area sizes and localities provided a means of assessment dependent upon a similar level of accessible information (i.e., available minutiae points). This was paramount in comparatively understanding the internal fingerprint in the context of current surface fingerprinting technology.

The following section exhibits the results obtained and provides a discussion thereof.

4 Results

On average, $45.4 \pm 9.6\%$ of C was interpolated to yield PC; this is due to the strong cluster membership requirement. Figure 8 conveys the performance analysis of the internal fingerprint extraction algorithm. Although the error metrics measured were never zero—on account of human error in G—there is a clearly evident region of stable high performance. The lowest MSE and H values are 21.65 and 147.78, respectively. In contrast, the work presented in Ref. 20 yielded a minimum MSE of 23.6 and similar H values. Furthermore, the region of stable performance evident in both Figs. 8(a) and 8(b) is more significant than the region observed in the earlier work.[20] These results are evidence of the robustness of the algorithm in detecting the internal fingerprint zone.

The internal and surface fingerprints' OCL scores are shown in Table 1, and the NFIQ scores are given in Fig. 9. Although the category 1 internal fingerprints had, on average, higher OCL scores than the surface fingerprints, both the category 2 and 3 internal fingerprints outperformed the surface fingerprints. The NFIQ pie charts demonstrate that the subjective division of internal fingerprints into
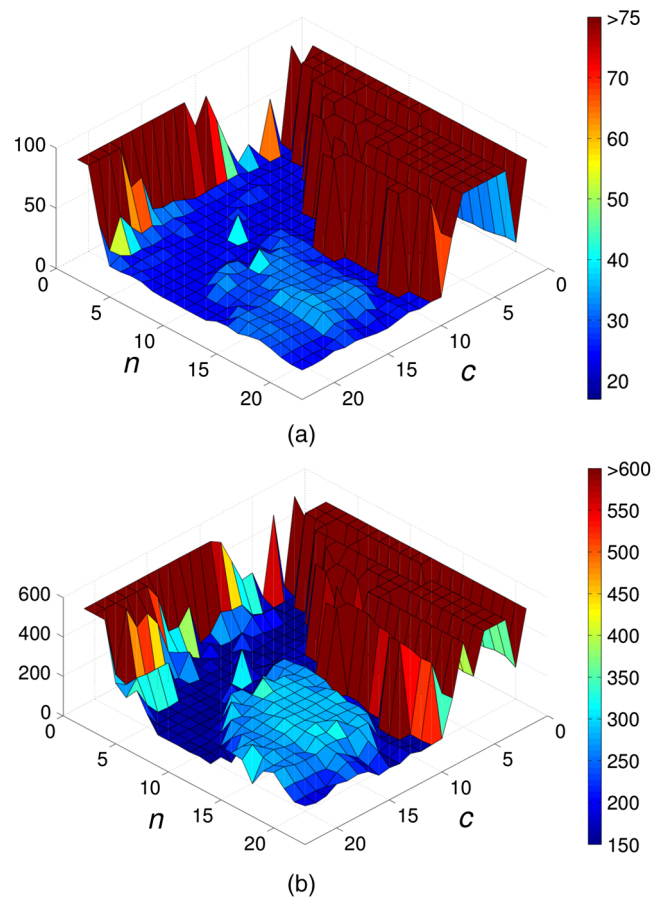
Fig. 8 Quantitative results comparing G and P over a range of $n = c = 2{:}23$. (a) The mean squared error results and (b) the H results.

three categories is dependent upon minutiae present (since the NFIQ score itself is dependent on this): 36.8% of the category 3 internal fingerprints had an NFIQ score of 1, compared to 22.2% and 5.6% for category 2 and 3 internal fingerprints, respectively. Furthermore, category 3 internal fingerprints outperformed the surface fingerprints in this regard, indicating superiority regarding minutiae available and the quality thereof.

Table 1 also presents the quantitative results of internal fingerprint to surface fingerprint and cross-correlation. The match scores were calculated as the mean (i.e., average match score when comparing an internal fingerprint to 16 surface counterparts) and maximum (i.e., the maximum score obtained considering all comparisons) scores. Both mean and maximum match scores were given as each is useful to fingerprint verification and identification processes. Figure 10 accompanies this, providing (a) the internal to surface correlation scores and (b) the internal cross-correlation scores, arranged in ascending order (denoted as the internal fingerprint index) by fingerprint category, NFIQ, and OCL. NIST states that a "true match" must have a score greater than 40; the dashed horizontal lines indicate this.

None of the category 1 fingerprints and only one of the category 2 fingerprints met the true match criteria, when compared to their surface counterparts. However, 74% of the category 3 fingerprints met this criterion. Thus, provided the OCT fingertip scan covers a sufficiently large area (15 mm × 15 mm, in this research) and the internal

Table 1 Average fingerprint match results for each internal fingerprint category.

Fingerprint type	OCL	Surface score (mean; max)	Cross score (mean; max)
Category 1	0.234 ± 0.074	$11.0 \pm 3.3; 18.0 \pm 6.1$	$59.3 \pm 35.3; 112.3 \pm 62.3$
Category 2	0.168 ± 0.028	$15.4 \pm 4.9; 24.9 \pm 9.3$	$65.8 \pm 34.8; 128.6 \pm 56.9$
Category 3	0.133 ± 0.056	$37.4 \pm 11.5; 61.6 \pm 32.1$	$57.9 \pm 48.8; 152.0 \pm 77.4$
Surface	0.182 ± 0.056	—	—
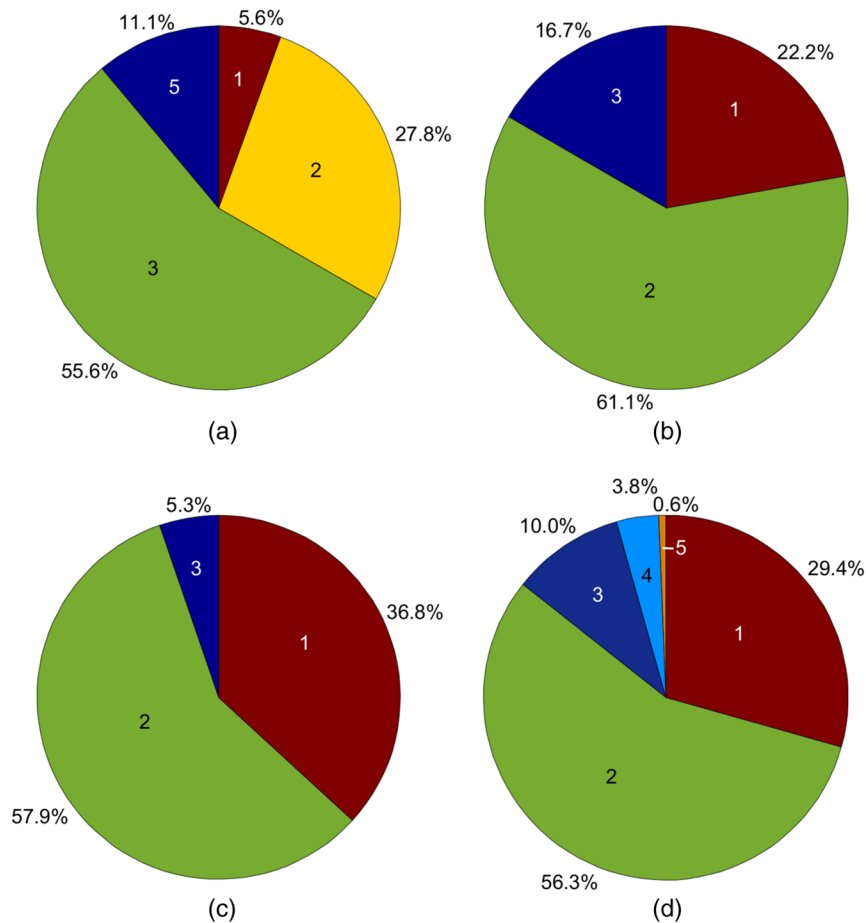
Fig 9 NFIQ scores. (a), (b), and (c) The NFIQ scores for category 1, 2, and 3 internal fingerprints, respectively. (d) The NFIQ scores for the full-sized corresponding surface fingerprints. The numbers inside the pie charts denote the NFIQ scores.

fingerprint is extracted using the algorithm presented here, the internal fingerprint can be integrated with current surface fingerprints. The top-right block of Fig. 10(a) is evidence of this. The dependence of the match score on the fingerprint quality (NFIQ) is evident in the upward trend exhibited in Fig. 10(a).

Ninety-six percentage of the internal fingerprints had a corresponding true match with another internal fingerprint. Therefore, a fingerprint database consisting only of internal fingerprints may perform well.

Figure 10(b) serves to exhibit internal fingerprint to surface and cross correspondence. Each conventional surface scan was compared to all others, of the same finger, in

order to assess the relative performance of internal fingerprints. The surface fingerprints yielded an average match score of 97 ± 76. Although the average surface-to-surface match score is well above the "true match" threshold, the high standard deviation present is evidence of inconsistency. These scores are comparable to the internal-to-internal match scores, but may seem to indicate that internal fingerprints do not perform sufficiently when a comparison is made between internal and surface fingerprints. However, the following factors must be taken into account:

1. A combination of the distortion induced by 3-D to 2-D planar extraction, "jitter" from the touchless OCT

(a)

(b)
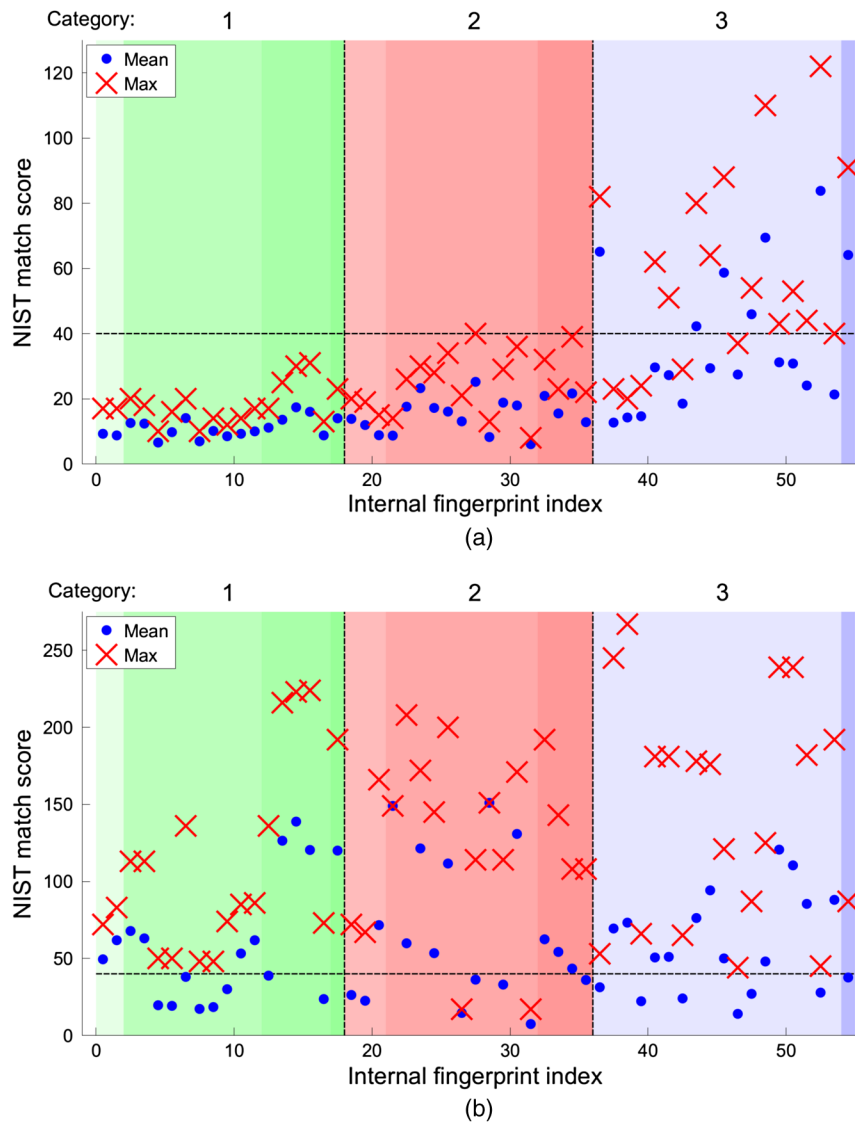
Fig. 10 Fingerprint match score results. (a and b) Encapsulate the NIST match scores for internal to surface and internal cross-correlation, respectively. The vertical divisions denote the three internal fingerprint categories. The vertical light to dark colors are the NFIQ scores. Within each vertical color bar, the fingerprints are ordered according to their orientation certainty level scores. The dashed horizontal line denotes a true match.

imaging, and surface fingerprint distortion have an effect on the surface to internal correlation. This needs to be addressed in future research. The category 3 internal fingerprint given in Fig. 11 shows significant jitter. The touchless OCT scans take approximately 20 s to complete and it is difficult for an individual to keep still for this period. Although it is difficult to attribute precise performance degradation owing to jitter, this must be dealt with in hardware design as a future task, but it is outside the scope of this research. Furthermore, future research will entail assessing various fingerprint matching algorithms with regard to invariance toward jitter.

2. The scan area size and localization are inconsistent between conventional surface and extracted internal fingerprints but consistent across all the surface scans. This is mainly owing to the difference in

acquisition procedure—a hardware constraint to be imposed in future research.

3. The characteristics of the surface scans are similar because they have the same or similar origins: the surface scanners. The OCT scan results in qualitatively different scans. This effect is difficult to quantify, but Fig. 11 shows examples of the three internal fingerprint categories with corresponding surface counterparts.

Figure 11 also shows that surface anomalies, such as wrinkles, are seen on the surface fingerprints, but not on the corresponding internal fingerprints; the internal fingerprint is resistant to damage due to everyday wear and tear.

It should be noted that the viability of this method for extracting internal fingerprints is independent of the
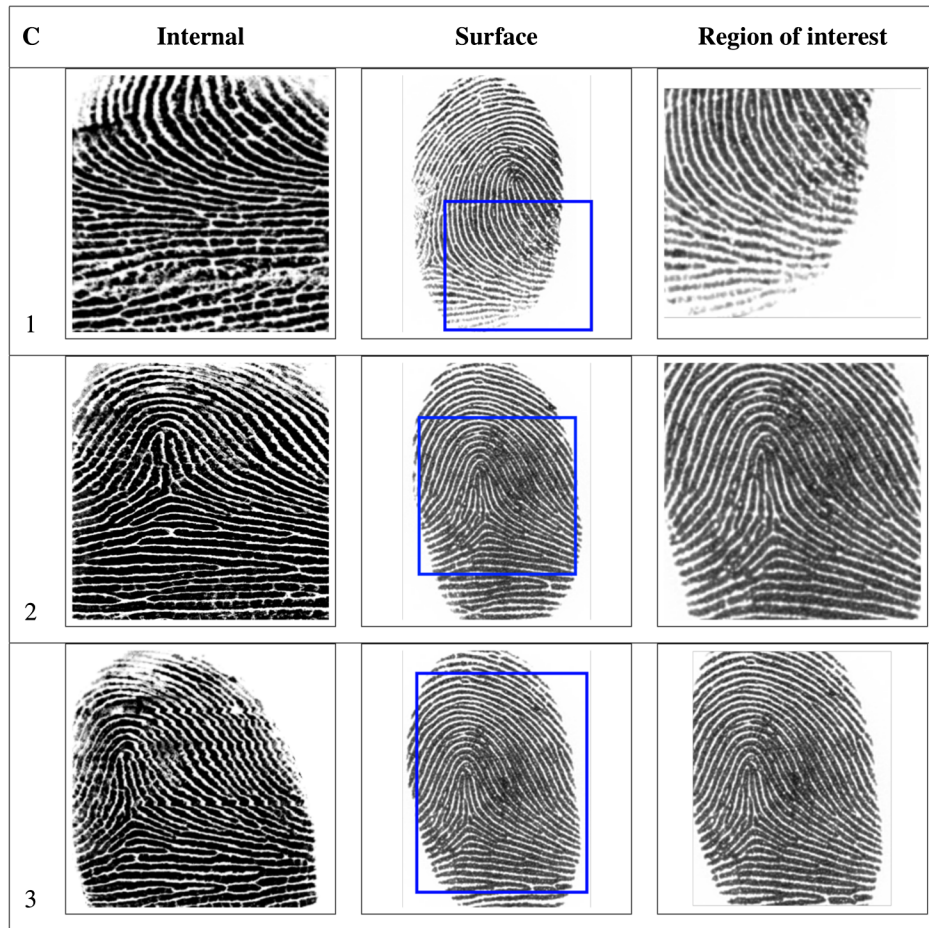
Fig. 11 Fingerprint category examples. *C* is indicative of fingerprint category. The category 1 internal fingerprint shown here encompasses a region overlapping with the joint/fold of the finger, thus it exhibits significant artifacts.

performance of the fingerprint itself (i.e., whether the imaged area is sufficient or not). The subjective classification of internal fingerprint categories used throughout this research exhibits the dependence of fingerprint performance on the scanned area itself. Therefore, for the internal fingerprint to be considered a viable replacement for current surface fingerprints, the scanned area must be sufficient.

To test this hypothesis, three surface fingerprints were obtained and cropped (denoted as SROI-fingerprints) for each internal fingerprint. Figure 12 exhibits the results
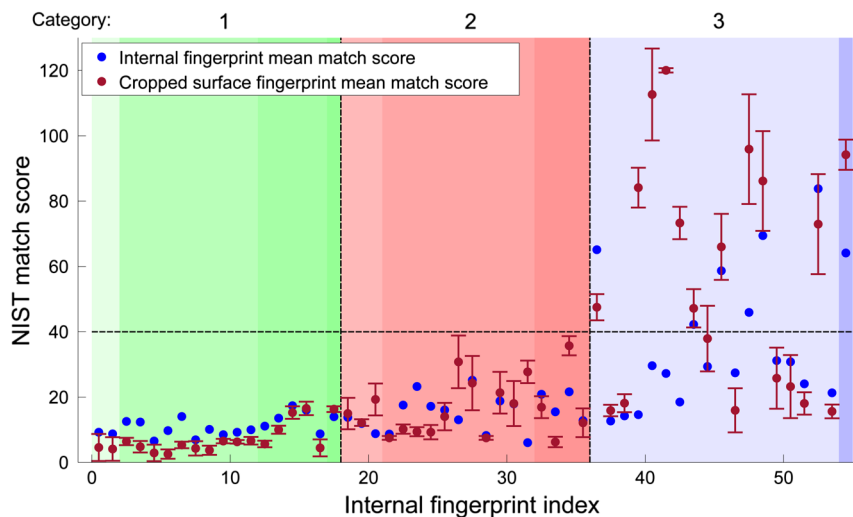
Fig. 12 Match performance results when compared to corresponding surface region. The (blue) dots show the score of the internal fingerprints. The (brown) dots and error boxes show the average corresponding surface-region-of-interest-fingerprints' scores and the standard deviation thereof, respectively.

obtained when comparing the internal fingerprints' performance to that of the SROI-fingerprints' performance. The majority of internal fingerprints performed either as well (within the measured error) or better than their corresponding SROI-fingerprints. Furthermore, the internal fingerprints had higher average match scores than their SROI-fingerprint counterparts' 63.6% of the time. Notwithstanding other factors biasing these results toward the SROI-fingerprints (such as different fingerprint distortion sources from internal and surface fingerprints), the internal fingerprints perform at a level comparable to the SROI-fingerprints.

The internal fingerprint could serve as a replacement for the surface fingerprint. However, the assessments provided in this section are not consistent with a traditional performance evaluation of a biometric system. Instead, they are to serve as an initial assessment of the internal fingerprint in the context of the performance of identical fingerprints extracted using traditional means (i.e., the surface scanner). In addition, this research endeavors to provide an advanced technique for fingerprint extraction from OCT fingertip scans. That said, the results shown in Fig. 12 give the most useful internal fingerprint performance indication. Future research will certainly entail error rate assessments using a large database of OCT scans and will provide a traditional biometric system evaluation.

Although not provided in this assessment, it would be useful to compare the internal fingerprint to a conventional surface fingerprint taken from an individual that has very poor fingerprints, very dry skin, or a skin disease (such as eczema). This will be carried out as future research.

The following section serves to draw conclusions regarding these results.

5 Conclusions

The internal fingerprint extraction algorithm proposed in this research has been shown to perform well regarding error minimization against a manually estimated internal fingerprint zone. The critical component of the algorithm is fuzzy c-means clustering. Since interpolation and image-enhancement-based fine-tuning procedures were employed, the stable region (regarding the number of data points and number of clusters) of high performance was large. The internal fingerprint zone was detected accurately.

Internal fingerprints were successfully extracted from 55 OCT fingertip volumes of varying spatial area and resolution. The OCL of the internal fingerprints was high when compared to their surface counterparts. When the captured internal fingerprints contain sufficient fingerprint details, they correlate well with their surface counterparts. Seventy-four percent of category 3 internal fingerprints had a true match with a surface counterpart. Furthermore, the cross-correlation of internal fingerprints was high, with 96% having a corresponding true match. Internal fingerprint cross-correlation was shown to be comparable to conventional surface fingerprint cross-correlation.

Three corresponding surface counterparts were obtained and cropped to provide a reference comparison. This was done to alleviate bias present due to the limitation of the OCT scanner in providing sufficient fingerprint area and locality. That is, the cropped surface counterparts contained a similar set of minutiae points to those contained in the internal fingerprints. This was necessary to quantitatively assess the performance of the internal fingerprint itself, rather than the area it constituted. The results of this testing showed that the internal fingerprint performed as well or better than cropped surface counterparts.

Procedural qualitative explanations of the algorithm were given throughout this work, and example internal fingerprints (with corresponding surface counterparts) were also given.

This work served to show quantitatively the internal to surface fingerprint correlation. Future work will be undertaken to show the performance of internal fingerprints through identification against existing fingerprint databases.

The work presented here detailed and tested an advanced technique for internal fingerprint extraction from touchless OCT fingertip scans. A 3-D to 2-D unwrapping[6] procedure is needed to reduce distortion and will be investigated in future work. Hardware constraints will be developed and employed, in a future work, to ensure the scanned area is consistently large and central enough to maximize fingerprint performance. In addition, error rate assessments will be carried out using a large dataset in order to comply with traditional biometric systems assessment.

References

1. T. Matsumoto et al., "Impact of artificial gummy fingers on fingerprint systems," *Proc. SPIE* **4677**, 275–289 (2002).
2. Y. S. Moon et al., "Wavelet based fingerprint liveness detection," *Electron. Lett.* **41**(20), 1112–1113 (2005).
3. C. Gottschlich et al., "Fingerprint liveness detection based on histograms of invariant gradients," in *2014 IEEE Int. Joint Conf. on Biometrics (IJCB)*, pp. 1–7, IEEE (2014).
4. S. Prabhakar, S. Pankanti, and A. K. Jain, "Biometric recognition: security and privacy concerns," *IEEE Secur. Privacy* **1**(2), 33–42 (2003).
5. A. W. Senior and R. M. Bolle, "Improved fingerprint matching by distortion removal," *IEICE Trans. Inf. Syst.* **84**(7), 825–832 (2001).
6. Y. Wang, D. L. Lau, and L. G. Hassebrook, "Fit-sphere unwrapping and performance analysis of 3D fingerprints," *Appl. Opt.* **49**(4), 592–600 (2010).
7. L. Coetzee and E. C. Botha, "Fingerprint recognition in low quality images," *Pattern Recognit.* **26**(10), 1441–1460 (1993).
8. S. Chikkerur, A. N. Cartwright, and V. Govindaraju, "Fingerprint enhancement using STFT analysis," *Pattern Recognit.* **40**(1), 198–211 (2007).
9. C. Champod et al., *Fingerprints and Other Ridge Skin Impressions*, CRC Press, Boca Raton, Florida (2004).
10. A. Fercher et al., *Optical Coherence Tomography*, John Wiley & Sons, Ltd., Hoboken, New Jersey (2006).
11. J. M. Schmitt, S. H. Xiang, and K. M. Yung, "Speckle in optical coherence tomography," *J. Biomed. Opt.* **4**(1), 95–105 (1999).
12. A. Bossen, R. Lehmann, and C. Meier, "Internal fingerprint identification with optical coherence tomography," *Photonic Technol. Lett.* **22**(7), 507–509 (2010).
13. M.-R. Nasiri-Avanaki et al., "Anti-spoof reliable biometry of fingerprints using en-face optical coherence tomography," *Opt. Photonics J.* **1**, 91 (2011).
14. F. Harms, E. Dalimier, and A. C. Boccara, "En-face full-field optical coherence tomography for fast and efficient fingerprints acquisition," *Proc. SPIE* **9075**, 90750E (2014).
15. G. Liu and Z. Chen, "Capturing the vital vascular fingerprint with optical coherence tomography," *Appl. Opt.* **52**(22), 5473–5477 (2013).
16. A. Zam et al., "Feasibility of correlation mapping optical coherence tomography (CMOCT) for anti-spoof sub-surface fingerprinting," *J. Biophotonics* **6**(9), 663–667 (2013).
17. R. Khutlang and F. V. Nelwamondo, "Novelty detection-based internal fingerprint segmentation in optical coherence tomography images," in *2014 Second Int. Symp. on Computing and Networking (CANDAR)*, pp. 556–559, IEEE (2014).

18. L. N. Darlow, S. S. Akhoury, and J. Connan, "Internal fingerprint acquisition from optical coherence tomography fingertip scans," in *2015 Third Int. Conf. on Digital Information, Networking, and Wireless Communications (DINWC)*, pp. 188–191, IEEE (2015).

19. S. S. Akhoury and L. N. Darlow, "Extracting subsurface fingerprints using optical coherence tomography," in *The Third Int. Conf. on Digital Information, Networking, and Wireless Communications*, IEEE (2015).

20. L. N. Darlow, J. Connan, and S. S. Akhoury, "Internal fingerprint zone detection in optical coherence tomography fingertip scans," *J. Electron. Imaging* **24**(2), 023027 (2015).

21. I. Sobel and G. Feldman, "A 3×3 isotropic gradient operator for image processing," in *Stanford Artificial Intelligence Project* (1968).

22. J. C. Bezdek, R. Ehrlich, and W. Full, "FCM: the fuzzy c-means clustering algorithm," *Comput. Geosci.* **10**(2), 191–203 (1984).

23. D. Garcia, "Robust smoothing of gridded data in one and higher dimensions with missing values," *Comput. Stat. Data Anal.* **54**(4), 1167–1178 (2010).

24. L. N. Darlow, S. S. Akhoury, and J. Connan, "A review of state-of-the-art speckle reduction techniques for optical coherence tomography fingertip scans," *Proc. SPIE* **9445**, 944523 (2015).

25. D. P. Huttenlocher, G. A. Klanderman, and W. J. Rucklidge, "Comparing images using the Hausdorff distance," *IEEE Trans. Pattern Anal. Mach. Intell.* **15**(9), 850–863 (1993).

26. David Tschumperlé, "GREYC'S magic for image computing," http://gmic.eu/ (November 2015).

27. U.S Department of Commerce, "National Institute of Standards and Technology," http://www.nist.gov/ (November 2015).

28. E. Lim, X. Jiang, and W. Yau, "Fingerprint quality and validity analysis," in *Proc. of Int. Conf. on Image Processing*, Vol. 1, pp. I–469, IEEE (2002).

Luke Nicholas Darlow is a researcher at Modelling and Digital Science, Council for Scientific and Industrial Research, South Africa. He obtained his BSc degree in computer science from Rhodes University and is passionate about pursuing avenues associated with fingerprint extraction from OCT fingertip scans.

James Connan is a senior lecturer at Rhodes University in Grahamstown, South Africa. He received his MSc degree in computer science from the University of Stellenbosch in 2004. His research interests include computer vision and image processing.